World Electric Vehicle Journal

MDPI

Article

Driving Control Strategy and Specification Optimization for All-Wheel-Drive Electric Vehicle System with a Two-Speed Transmission

Jeonghyuk Kim [1], Jihyeok Ahn [1], Seyoung Jeong [1], Young-Geun Park [1], Hyobin Kim [1], Dongwook Cho [2] and Sung-Ho Hwang [1,*]

[1] Department of Mechanical Engineering, Sungkyunkwan University, 2066 Seobu-ro, Suwon 16419, Republic of Korea; jungjjang44@naver.com (J.K.); ahnkevin0@g.skku.edu (J.A.); nasy960@skku.edu (S.J.); biee00m@naver.com (Y.-G.P.); illusosmile@naver.com (H.K.)

[2] Department of Intelligent Robotics, Sungkyunkwan University, 2066 Seobu-ro, Suwon 16419, Republic of Korea; dw0313@g.skku.edu

* Correspondence: hsh0818@skku.edu

Abstract: Equipping electric vehicles with a two-speed gearbox allows for achieving high torque and maximum speed through appropriate gear ratio adjustments. Additionally, tuning motor operating points to efficient zones, considering energy efficiency, significantly enhances the vehicle's overall performance. This paper presents an AWD system configuration method, integrating a two-speed transmission to improve energy efficiency and driving performance through front and rear motor torque distribution and powertrain specification optimization. Based on vehicle simulations conducted using MATLAB/Simulink, a strategy for torque distribution between the front/rear axles was established using fuzzy logic, considering energy efficiency and driving stability. Furthermore, a multi-objective optimization was performed using a surrogate model trained through MATLAB parallel simulations. When the optimization results were applied to various vehicle specifications, it was observed that energy efficiency was improved, and acceleration performance was increased compared to a baseline vehicle without optimization.

Keywords: AWD electric vehicle; two-speed transmission; torque distribution; surrogate model; multi-objective optimization

Citation: Kim, J.; Ahn, J.; Jeong, S.; Park, Y.-G.; Kim, H.; Cho, D.; Hwang, S.-H. Driving Control Strategy and Specification Optimization for All-Wheel-Drive Electric Vehicle System with a Two-Speed Transmission. *World Electr. Veh. J.* **2024**, *15*, 476. https://doi.org/10.3390/wevj15100476

Academic Editors: Joeri Van Mierlo, Myoungho Sunwoo and Namwook Kim

Received: 13 September 2024
Revised: 14 October 2024
Accepted: 17 October 2024
Published: 19 October 2024

1. Introduction

Due to global environmental regulations, countries are strengthening regulations on internal combustion engine vehicles, and there is a notable trend towards the transition to electric vehicles (EVs). Consequently, various existing internal combustion vehicles are converted to electric vehicles [1–3]. However, electric vehicles face issues of short driving ranges due to low energy density, and recently, consumers have had higher expectations for the driving performance of electric vehicles. Against this backdrop, many automobile manufacturers focus their research and development efforts on meeting these dual demands [4].

A recent solution to these problems proposes the integration of a two-speed transmission in the EV layout. Typically, the fixed-ratio gear reducer installed in electric vehicles provides sufficient acceleration performance even at low speeds due to the torque characteristics of electric motors, and it is widely used due to its simple design and highly efficient operation within a specific rotational speed range of the motor. However, fixed-ratio gear reducers limit the dynamic performance of electric vehicles and reduce the utilization of the motor's high-efficiency range, thus hindering efficient driving [5]. A two-speed transmission can satisfy both high initial drive torque and high top speeds. An appropriate shifting strategy allows for controlling motor operation points, enhancing motor driving

efficiency [6,7]. For instance, Huang et al. [8] demonstrated the advantages of a two-speed transmission by comparing motor operation points with a fixed-ratio reducer and changes in vehicle driving performance according to the gear ratio under the European New Driving Cycle (NEDC). Janulin et al. [9] reduced the energy consumption of a vehicle by optimizing the gear ratio parameters in actual traffic cycles.

The All-Wheel-Drive (AWD) layout can be utilized to enhance the driving performance of electric vehicles. The AWD system delivers power to all wheels, providing superior driving performance on slippery roads and rough terrains, thereby improving driving stability and traction capabilities [10]. The multi-motor configuration of this system allows for appropriate torque distribution to the front and rear motors, which enhances driving performance and energy efficiency. In this context, Dizqah et al. [11] proposed a rapid and parameterized torque distribution strategy for four-wheel drive electric vehicles to increase energy efficiency. Cao et al. [12] suggested a method to improve vehicle energy consumption and wheel slip ratio performance through multi-purpose optimal torque distribution in four-wheel drive electric vehicles.

Therefore, the new structure equipped with a two-speed gearbox in the AWD layout has the advantage of satisfying electric vehicle driving efficiency, vehicle power performance, and driving stability through appropriate shift strategies and torque distribution. Currently, many studies are being conducted related to this. However, as the layout becomes more complex, it is necessary to consider that the design time can increase due to the many powertrain specification variables that must be considered during the vehicle design phase. To address this, researchers have recently presented methods to optimize various powertrain structures and pre-select component specifications to reduce design time. For example, Kim et al. [13] presented a method to determine the optimal gear ratio that satisfies the dynamic performance of hybrid electric vehicles while minimizing energy consumption. Nguyen et al. [14] proposed an energy management strategy through gear shift scheduling using a dual-loop optimization algorithm to explore motor capacity and gear ratios.

Related prior studies primarily focus on optimizing gear ratios to improve the performance of electric vehicles, and there are few studies on the simultaneous optimization of motor specifications and shift maps. Individually optimizing the gear ratio, motor specifications, and shift maps has the advantage of simplifying the optimization process. However, this method does not reflect the interaction between these elements. Therefore, it cannot guarantee the system's optimal performance. Additionally, the design of objective functions is crucial when performing multi-objective optimization. However, designing objective functions based on formulas can result in a lack of credibility in the solutions derived from optimization, as they fail to fully reflect vehicle modeling. Therefore, to address these issues, the main contributions of this paper are summarized as follows:

(i) A method is presented for the simultaneous optimization of motor specifications, reduction ratios, and shift maps, considering torque distribution strategies for both front and rear wheels, which is expected to maximize vehicle performance;
(ii) An objective function was designed by training electric vehicle simulation data using deep learning for application in multi-objective optimization. This approach enhances the credibility of selecting optimal specifications for the AWD EV powertrain.

Firstly, the paper proposes a method that integrates motor torque distribution strategies with optimization techniques to fully utilize the characteristics of AWD EVs equipped with two-speed gearboxes. Changes in component specifications, such as motor specifications and reduction ratios, result in variations in the torque distribution ratio map to maximize energy efficiency. Consequently, a variable torque distribution ratio 2D Look-up Table, adjusted for various input parameters (maximum motor torque and power, front and rear reduction ratios, shifting speeds), is applied in the simulator. The simulation outputs, such as State of Charge (SOC) variations and acceleration times, are then used for optimization. This method offers the advantage of producing solutions close to the system's optimal performance by considering major powertrain component specifications

simultaneously. An additional consideration is that focusing the torque distribution strategy solely on energy efficiency often concentrates torque on one motor, which can reduce vehicle stability in special situations like rapid acceleration or deceleration. In response, the paper presents an integrated torque distribution methodology that can adjust between a torque distribution strategy focused on energy efficiency and one focused on straight driving stability based on Fuzzy Control.

Additionally, the objective functions used in this study for multi-objective optimization are energy consumption and acceleration performance. However, setting up objective functions based on formulas to predict energy consumption and acceleration performance for complex vehicle structures with a transmission in the AWD layout is quite challenging. This is due to elements like motor efficiency maps, which have nonlinear solid characteristics, making output prediction difficult. Therefore, in this paper, we use deep learning to create a surrogate model that emulates electric vehicle simulations. Through this model, two objective functions—one for energy consumption (SOC variations) and another for acceleration performance (0–96 kph acceleration time)—are designed and applied to multi-objective optimization.

The structure of this paper is as follows: Section 2 describes the methodology for modeling AWD vehicles based on MATLAB/Simulink (https://www.mathworks.com/), including explanations and result graphs for shift logic to prevent torque holes and shift shocks. Section 3 discusses the motor torque distribution strategies required for optimization and explains how energy efficiency and driving stability were simultaneously considered using Fuzzy Control. Section 4 focuses on the main content of this paper, explaining the method of using an Artificial Neural Network (ANN) to emulate electric vehicle simulations with torque distribution strategies and the approach for deriving optimal solutions through multi-objective optimization based on the Non-Sorted Genetic Algorithm-II (NSGA-II). Section 5 presents and discusses the simulation results. Finally, Section 6 summarizes the key conclusions.

2. AWD Vehicle Modeling with Two-Speed Transmission

As shown in Figure 1, an AWD electric vehicle equipped with one motor on each front and rear axle was developed using MATLAB/Simulink. The powertrain consists of a battery, Vehicle Control Unit (VCU), two motors, gears connected to the front axle motor, and a two-speed transmission connected to the rear axle motor. Section 2.2 provides detailed descriptions of each module.

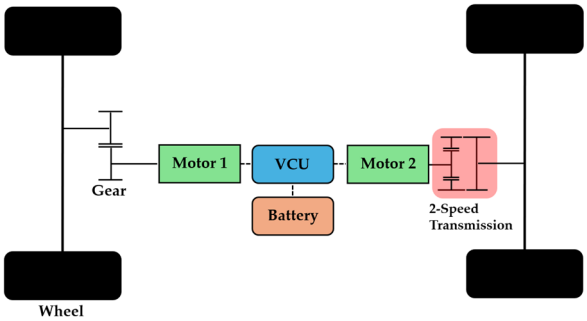

Figure 1. Schematic Diagram of 2-Speed Transmission AWD Vehicle Powertrain Structure.

2.1. Parameters of the Target Vehicle

The paper considers three types of vehicle specifications: Sedan, SUV (Sport Utility Vehicle), and SUV equipped with a trailer. Table 1 displays the key parameters used in the system and the optimization parameters. Moreover, Table 2 displays the vehicle performance indicators.

Table 1. Target vehicle key parameters.

Item	Value [Unit]
Vehicle mass (Sedan/SUV/SUV-Trailer), m	2265/2728/5803 [kg]
Base motor power, P/Maximum torque, T	92 [kW]/230 [Nm]
Base motor max speed, ω_{max}/motor base speed, ω_{base}	20,000 [RPM]/3820 [RPM]
Battery capacity, Q_n	77.4 [kWh]
Initial front gear ratio, i_f	10.65 [-]
Initial rear 1st/2nd gear ratio, i_{r1}/i_{r2}	14 [-]/6 [-]

Table 2. Electric vehicle performance indicators.

Indicators	Value [Unit]
Maximum vehicle speed (Sedan/SUV/SUV-Trailer)	225/170/128 [km/h]
Maximum climbing grade	60 [%]
Acceleration time (0~96 km/h)	4.1/5.0/20.0 [s]

2.2. AWD Electric Vehicle Model-Based Simulation

The backward simulation was selected to optimize electric vehicle components and system specifications. This approach calculates the required power of the vehicle from a speed profile, not dynamic state variables. It allows for establishing optimal energy management strategies among various components while shortening simulation time [15]. Additionally, it enables rapid iterative simulations, contributing to time savings in the optimization process. The structure of the backward simulation is shown in Figure 2.

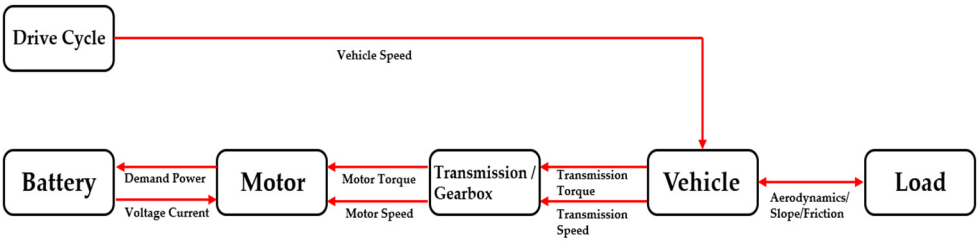

Figure 2. Backward simulation structure.

The backward simulation comprises several subsystems, and the description of each subsystem is as follows:

(1) Driving Cycle and Vehicle: Vehicle speed is calculated based on the driving cycle, and from this speed, driving resistance is computed to determine the vehicle-level output force. The calculation for vehicle-level output force is as follows [16].

$$F = m \cdot \frac{dv}{dt} = \frac{T}{r_D} - \left(\mu_r mg cos\theta + \frac{1}{2} C_D \rho_a A v^2 + mg sin\theta \right) \quad (1)$$

where F is the vehicle-level output force; v is the vehicle speed; T is the total (front/rear) wheel torque; r_D is the tire radius; μ_r is the rolling resistance coefficient; C_D is the air drag coefficient; ρ_a is the air density; A is the windward area; and θ is the climbing gradient.

(2) VCU: Based on the vehicle-level required torque, values for Accel Pedal (AP) and Brake Pedal (BP) are calculated. Then, the torque distribution logic derives the required torque levels for the front and rear motors. Estimating vertical forces for the front and rear axles is also conducted simultaneously. The formula for estimating vertical forces is as follows.

$$F_{zf} = mg \cdot \left(\frac{l_r}{L} - \frac{h}{L} \cdot \frac{a}{g} \right) \quad (2)$$

$$F_{zr} = mg \cdot \left(\frac{l_f}{L} + \frac{h}{L} \cdot \frac{a}{g} \right) \tag{3}$$

where F_{zf}, F_{zr} are normal force of front/rear wheel; l_f, l_r are the front/rear distance from the center of gravity; L is the total wheelbase; h is the height of the center of gravity; and a is the vehicle acceleration.

(3) Motor: Motor efficiency is determined based on the required motor torque and speed calculated by the VCU. The motor efficiency map was adapted by transforming the x- and y-axis scale of the reference motor's efficiency map. Section 4 discusses the efficiency map scaling method in detail. Then, considering the motor efficiency and the battery's Open Circuit Voltage (OCV), the battery current is calculated. The speed of the rear motor is inputted, considering the transmission's first and second-gear ratios. The calculation for the battery current during motor charge and discharge, considering motor torque, speed, and efficiency, is as follows.

$$I_d = \left(\frac{T_1 \omega_1}{\eta_1} + \frac{T_2 \omega_2}{\eta_2} \right) \cdot \frac{1}{V_t} \tag{4}$$

$$I_c = (T_1 \omega_1 \eta_1 + T_2 \omega_2 \eta_2) \cdot \frac{1}{V_t} \tag{5}$$

where I_d, I_c are the battery current during motor(charge/discharge); ω is the motor speed; η is the motor efficiency; and V_t is the voltage applied to the motor.

(4) Battery: The SOC is calculated using the Open Circuit Voltage and the required battery current. Then, the voltage applied to the motor is computed using the SOC and the circuit voltage values. The battery model utilizes a first-order R equivalent circuit model, as shown in Figure 3. The formulas for calculating the motor applied voltage and SOC are as follows:

$$V_t = I \cdot R_{int} - V_{oc}(SOC) \tag{6}$$

$$SOC(t) = SOC(t-1) + \frac{I(t)}{Q_n} \Delta t \tag{7}$$

where $R_{int} (= R_0)$ is the battery's internal resistance; SOC is the state of charge of battery; $V_{oc}(SOC)$ is the open circuit voltage based on SOC; and $I(t)$ is the battery current.

(5) Transmission: Unlike internal combustion engine vehicles, electric cars benefit from the torque-speed characteristics of electric motors, which provide high torque at low speeds and maintain constant power across an extended speed range. Due to these characteristics, electric vehicles can achieve the necessary performance with fewer gears [17]. Transmission modeling can consider various structures, and in this paper, a dog clutch-type transmission system was selected. The dog clutch is simple in structure and excellent in power transmission efficiency, making it suitable for electrified transmission systems. Due to these characteristics, it can be utilized in two-speed transmission systems.

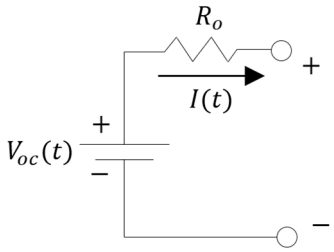

Figure 3. Equivalent circuit of internal resistance model.

2.3. Gear Shift Mechanism

Due to simulation time constraints, a detailed transmission dynamic model was not implemented. Instead, the system was structured to shift gears based on different states aligned with the gear change process. To minimize shift shocks, a 'speed synchronization' process was included where the motor speed in neutral matches the gear's speed to be engaged next [17]. Below is the gear change process divided by states.

- State 1. Torque Phase and Gear Neutral: When a gear shift command is issued, the torque of the rear motor is controlled to zero. Simultaneously, the torque of the front motor is compensated to maintain maximum total torque [18]. After the torque phase, the control shifts to neutral in the transmission.
- State 2. Speed Synchronization: Control the motor to the target speed range to mitigate shocks during the clutch engagement due to speed changes in the dog clutch gear when shifting. The speed synchronization phase ends when the difference between the target and motor speeds is less than or equal to 1 rad/s. The formula to calculate the motor speed when in neutral is as follows.

$$\omega = \int \dot{\omega} dt = \int \frac{T}{J} dt \tag{8}$$

  where ω is the rear motor speed in a neutral state; T is the rear motor torque in a neutral state; and J is the moment of inertia of the motor, shaft, and clutch.
- State 3. Gear Engagement and Torque Phase: Engage the dog clutch actuator and normalize the torque distribution between the front and rear motors.

Figure 4 illustrates the speed synchronization process of the rear motor in a neutral state. First, the target reference speed for the rear motor shift is calculated using the vehicle speed and the current rear gear ratio (first/second gear). Then, motor torque is output through the speed synchronization process based on a PI controller in the neutral state. The motor torque is converted to speed using Equation (8) and fed back into the PI controller. When the difference between the reference speed and the rear motor speed in neutral falls below 1 rad/s, the shift end signal changes, and the speed synchronization process ends.

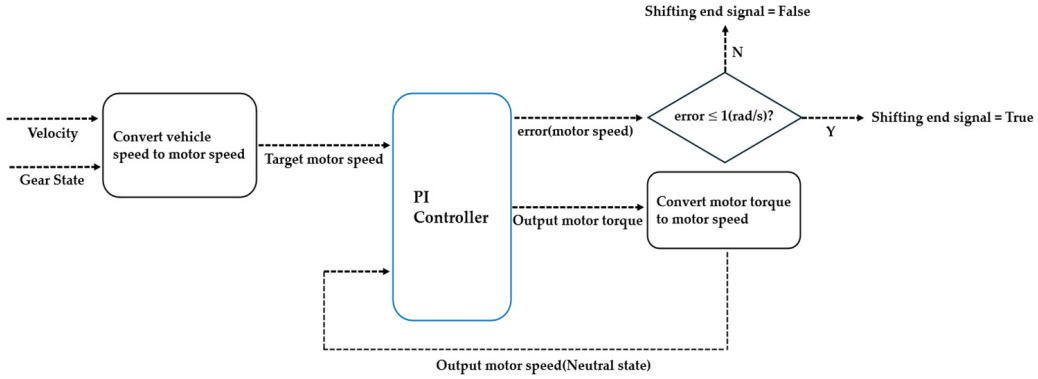

Figure 4. Schematic Diagram of Neutral State Speed Control Module.

Figure 5 shows the results of rear motor speed control and torque values in neutral state during upshifting and downshifting when a two-speed shift logic is applied. The sky-blue area represents the gear-neutral state in Figure 5.

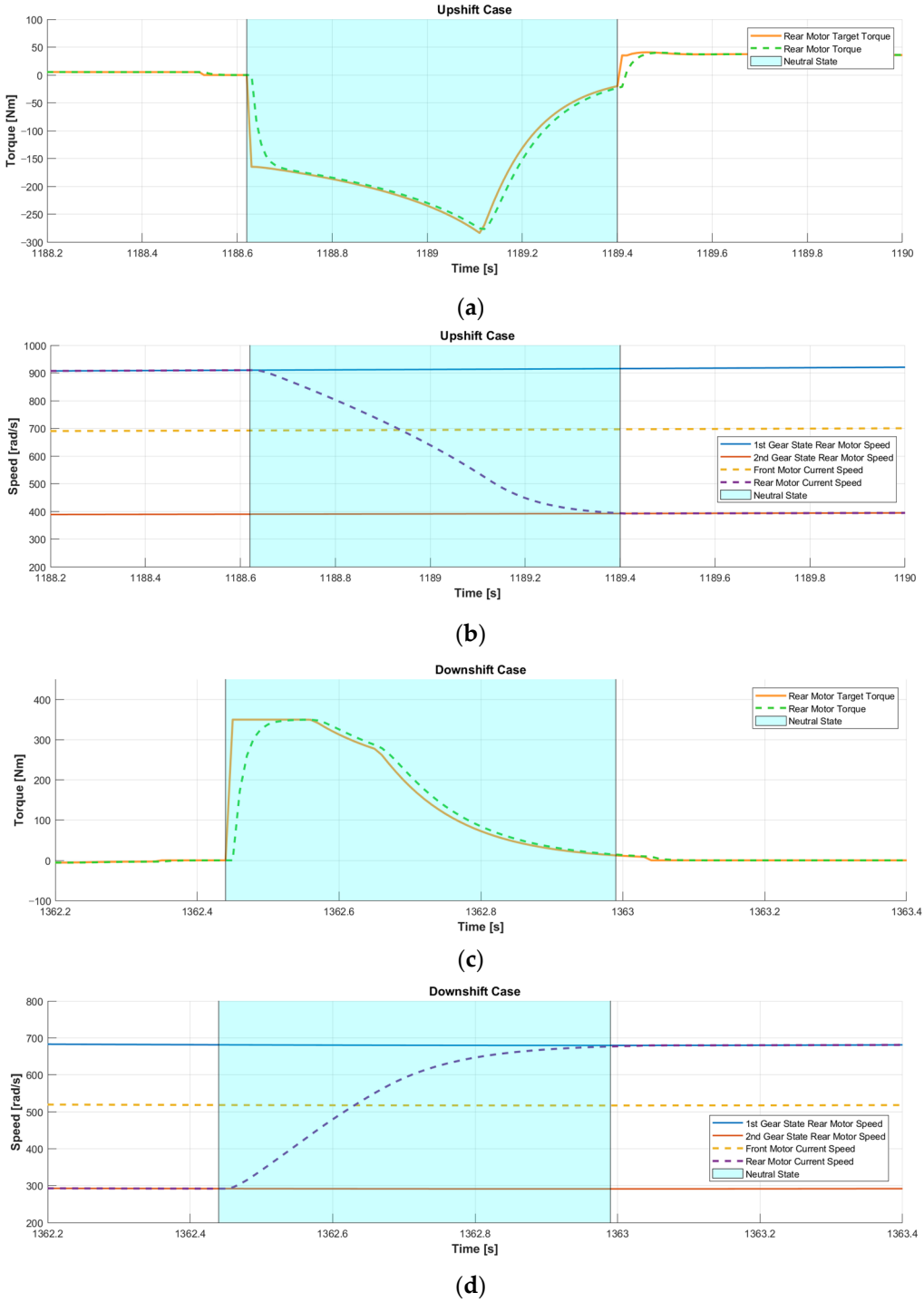

Figure 5. (**a**,**c**) Target torque and torque results for the rear motor in a neutral state (Upshift case, Downshift case); (**b**,**d**) target motor speeds for each gear and motor speeds of front/rear motor in a neutral state (Upshift case, Downshift case).

3. Integrated Torque Distribution Logic

In AWD systems equipped with front and rear motors, appropriate motor torque distribution can enhance energy efficiency. However, focusing solely on energy efficiency can lead to unstable vehicle behavior. Therefore, a torque distribution strategy based on efficiency maps and vertical force-based optimal braking force has been adopted. This strategy is regulated using Fuzzy Control to adjust the torque distribution dynamically [19].

3.1. Detailed Torque Distribution Logic

3.1.1. Energy Efficiency-Based Torque Distribution Strategy

Once the specifications for the front and rear motors are determined, front and rear motor efficiency maps can be generated based on the baseline motor efficiency map. Once the front and rear motor efficiency maps are established, the combined battery consumption power for the front and rear can be calculated when specific wheel torque and speed are input. To create a 2D Look-up Table focused on energy efficiency for front and rear torque distribution ratios, a global search algorithm was devised to store the distribution ratios that yield the minimum combined battery consumption power within the specified wheel torque and speed range. The corresponding Flow Chart and the 2D Look-up Table derived through the global search algorithm are illustrated in Figures 6 and 7, respectively. In Figure 7, as the color changes from blue to yellow, it indicates that the torque ratio is approaching 1.

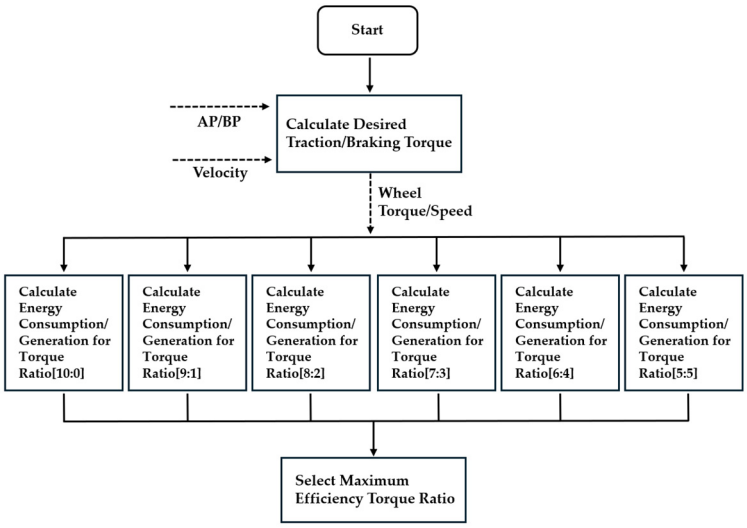

Figure 6. Flow Chart of the Strategy for Optimizing Driving Efficiency (Adapted from Ref. [19]).

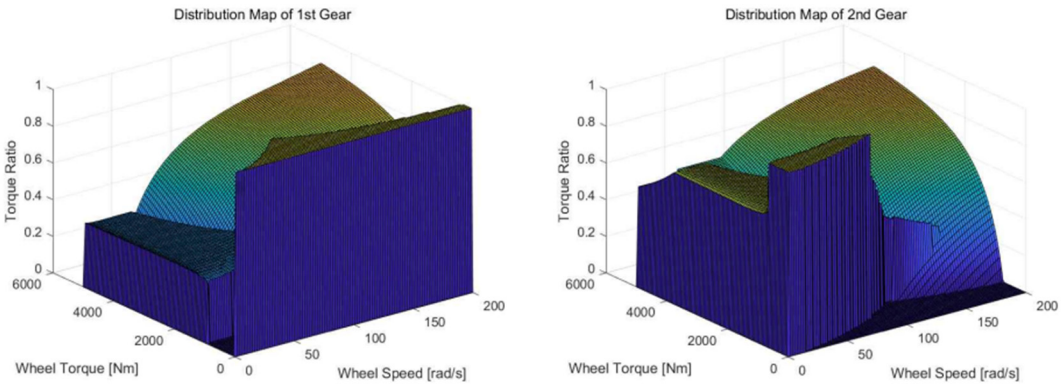

Figure 7. Distribution Map of 1st/2nd Gear.

3.1.2. Vertical Force-Based Torque Distribution Strategy

When a vehicle's torque distribution strategy focuses solely on efficiency, there is a potential to lose driving stability in specific situations, such as rapid acceleration or deceleration. This occurs because the motor's operating points tend to be positioned within high-efficiency areas, causing the required torque to concentrate on the front or rear wheels. Therefore, vertical forces based on the vehicle's acceleration have been calculated and

used to further consider torque distribution. The front wheel torque distribution ratio is expressed using Formulas (2) and (3) as follows.

$$Front\ Torque\ Ratio = \frac{F_{zf}}{F_{zf} + F_{zr}} \tag{9}$$

This formula minimizes tire slip by allocating more torque to the wheels with higher vertical forces. It is intuitively understood.

3.2. Integration of Torque Distribution Based on Fuzzy Logic

An appropriate mix between the two specific torque distribution strategies mentioned earlier is necessary for efficient vehicle operation. Therefore, the two distribution strategies are adjusted based on the driver's acceleration and deceleration demands. To more accurately determine the driver's acceleration and braking requirements, alpha (α) has been defined.

$$\alpha = \frac{v}{AP\ or\ BP} \tag{10}$$

Alpha represents the value obtained by dividing vehicle speed by the pedal value, and the magnitude of α and vehicle speed can be used to determine the driver's intentions for cruising and acceleration/deceleration. For example, if the vehicle speed is low and the AP value is high, α will decrease, indicating a high demand for acceleration by the driver. Conversely, if the vehicle speed is high and the AP value is low, α will increase, indicating a high demand for cruising by the driver.

Considering this, the driver's driving requirements based on the current vehicle state can be generated into a 2D Look-up Table using Fuzzy Logic. To create the map, the first step was to set up a scenario where the vehicle accelerates from 0 km/h to a predetermined speed and maintains it. Subsequently, this scenario was executed in a simulation environment at various speeds to monitor the changes in α, and α threshold values for acceleration and cruising at specific speeds were derived. Using the speed and α threshold values, an input membership function was designed within the fuzzy logic system to process the input data. This membership function receives input data (speed, α) and outputs a value (ranging from 0 to 1) that indicates how much the data belongs to a logical set. This output value was then used to create a 2D Look-up Table, as shown in Figure 8. Like Figure 7, in Figure 8, as the color changes from blue to yellow, it indicates that the reflection rate approaches 1.

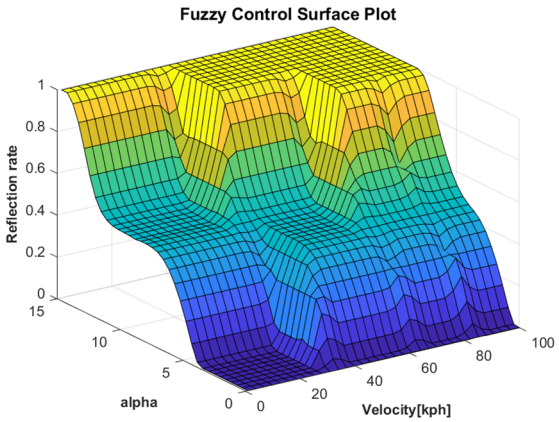

Figure 8. Fuzzy Control Surface Plot.

In the surface plot of Figure 8, the output of the control value represents the ratio of influence between the energy efficiency-based torque distribution strategy and the vertical force-based torque distribution strategy. An output close to 1 indicates a higher preference for cruising, emphasizing the efficiency-centric distribution strategy. Conversely, a value

close to 0 signifies a greater need for acceleration, favoring a strategy that allocates more vertical force to the front and rear wheels. Figure 9 diagrammatically shows the method of adjusting between these two distribution strategies based on the previously described fuzzy logic. In the Fuzzy Control Surface Plot, as the color changes from blue to yellow, it indicates that the reflection rate approaches 1.

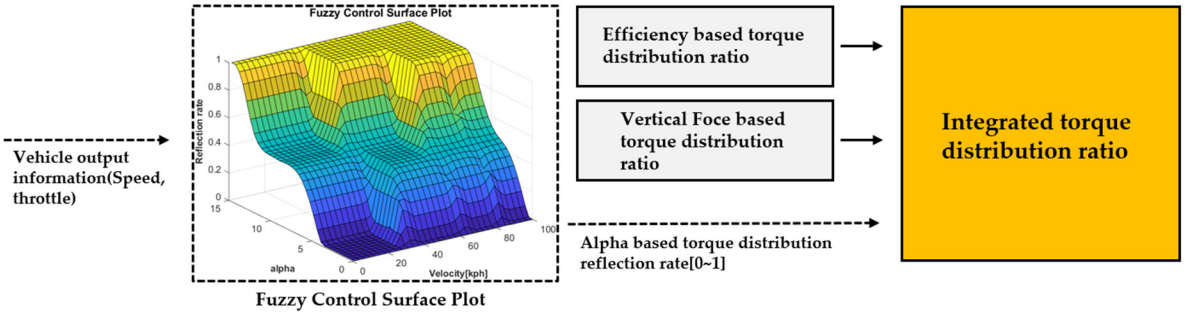

Figure 9. Schematic of torque distribution integration logic.

Unlike driving conditions, friction braking, and regenerative braking are considered simultaneously in braking scenarios, necessitating additional logic to manage the distribution between these two types of braking [20,21]. The general objective is to maximize the use of regenerative braking. When the total braking torque at the front and rear wheels exceeds the regenerative braking torque, the excess torque is transferred to friction braking. Here, Fuzzy Logic is used to adjust between cases that maximize regenerative braking (left side) and those that focus on the ideal braking force for the front and rear wheels (right side), as shown in Figure 10. For instance, if the BP value is high and changes abruptly, the distribution is adjusted closer to the ideal braking force, considering the vertical loads on the front and rear wheels. Conversely, if the vehicle behavior is deemed stable, the distribution shifts towards maximizing regenerative braking. Additionally, using regenerative braking while the vehicle is traveling at low speeds can negatively affect ride comfort. Therefore, the amount of regenerative braking has been linearly reduced in low-speed situations.

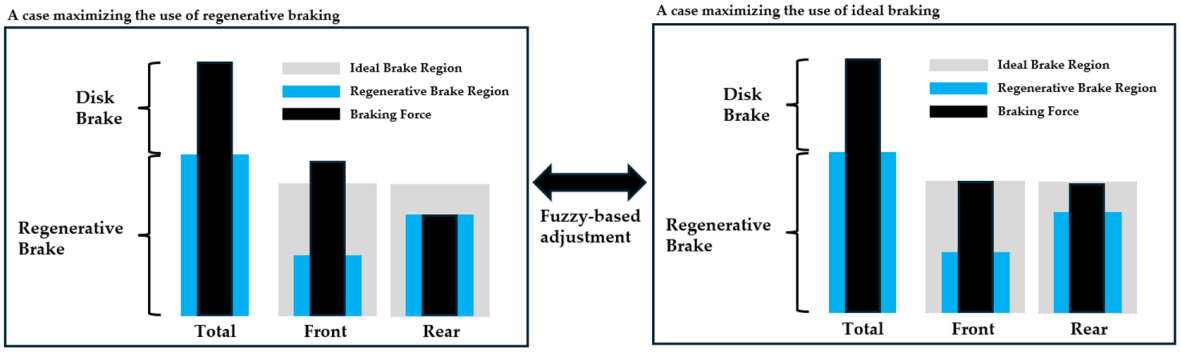

Figure 10. Schematic diagram of braking force distribution logic between friction and regenerative braking.

Figures 11 and 12 display the ideal and actual braking forces for the front and rear wheels during the WLTP (Worldwide Harmonized Light Vehicles Test Procedure) cycle, both with and without applying fuzzy logic. Without fuzzy logic, there was a tendency for braking force to concentrate on the rear wheels. However, after applying fuzzy logic, the ideal and actual braking forces for the front and rear wheels were closely aligned.

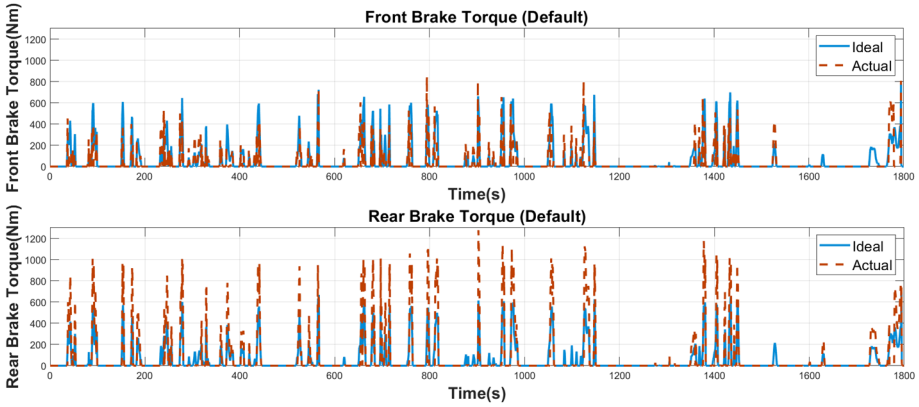

Figure 11. Front/rear ideal braking force (blue) and actual braking force (orange) (before applying Fuzzy Logic).

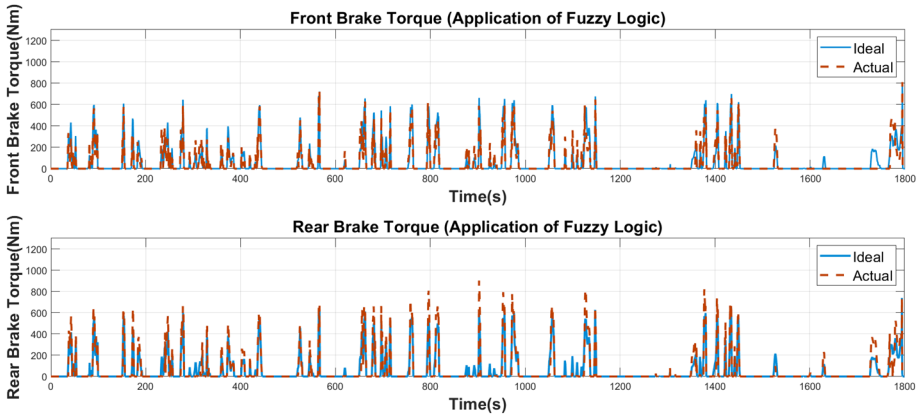

Figure 12. Front/rear ideal braking force (blue) and actual braking force (orange) (after applying Fuzzy Logic).

4. Powertrain Specification Optimization Strategy

The paper adopts a strategy incorporating torque distribution into the powertrain specification optimization strategy to maximize the improvement of vehicle power performance and energy efficiency. Figure 13 shows the flowchart of the overall optimization strategy.

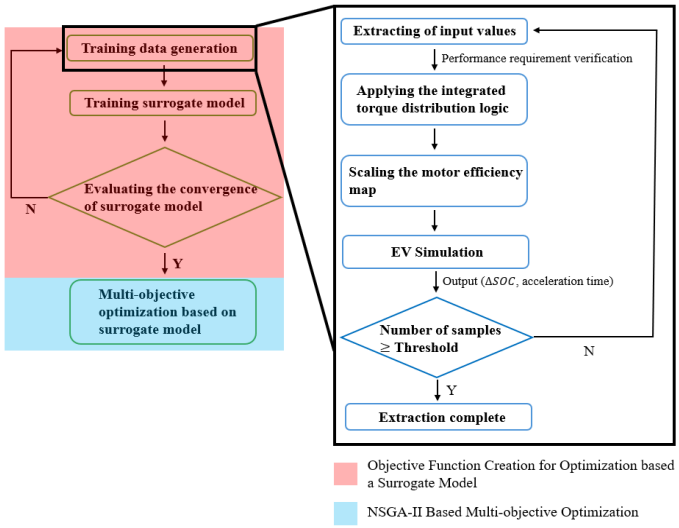

Figure 13. Flowchart of the overall optimization process.

The overall optimization process is divided into two main parts. Section 4.1 discusses the design method of the optimization objective function based on surrogate models, and Section 4.2 covers the extraction of optimal solutions based on multi-objective optimization. This study utilizes the NSGA-II algorithm, which is well known for effectively solving multi-objective optimization problems in various engineering fields [22]. However, this optimization algorithm requires excessive iterative calculations to determine the optimal solutions. An Artificial Neural Network (ANN) model has been trained to emulate a complex EV model to address the computational costs of optimization and is used as a surrogate model for the vehicle simulator [23].

Initially, training data are required to train the surrogate model. The part surrounded by the right black box represents the process of generating training data. Once input variables are extracted through an adaptive sampling process, corresponding torque distribution maps, and motor efficiency maps are created. After these preliminary steps, electric vehicle modeling-based simulations are performed, and outputs such as SOC changes (ΔSOC) and acceleration times (t_{acc}) are extracted. This process is repeated until the data size meets or exceeds a predefined threshold, at which point it transitions to the surrogate model training phase. Subsequently, deep learning is used to train the surrogate model, and convergence is evaluated. Finally, after the convergence assessment, NSGA-II multi-objective optimization is conducted to derive optimal solutions.

4.1. Objective Function Creation for Optimization Based on a Surrogate Model

A surrogate model is a model that can simplify and substitute for costly and complex simulations widely used across various fields [24,25]. The primary purpose of this model is to quickly and cost-effectively predict outputs based on input data. Surrogate models are constructed using statistical or machine learning techniques, such as polynomial regression, artificial neural networks, and Gaussian process regression. Various input variables are fed into backward simulations to build the dataset necessary for model fitting. These simulations consist of multiple subsystems, resulting in solid nonlinearity in the output values. Artificial neural networks, which can effectively learn complex data patterns and capture interactions between input variables, are well suited for modeling nonlinear relationships, making them ideal for constructing surrogate models.

4.1.1. Neural Network Training: Description of Input and Output Variables

In this paper, the input variables for neural network training consist of the maximum torque and power of the front and rear motors, the front axle reduction ratio, the rear axle's first and second reduction ratios, and the shifting speed. The motor efficiency map must also change accordingly as the motor-related variables change. Therefore, a new motor efficiency map was generated by altering the x and y-axis scales based on the reference motor efficiency map matching the altered motor specifications. Figure 14 shows an example of creating a motor efficiency map from the reference motor.

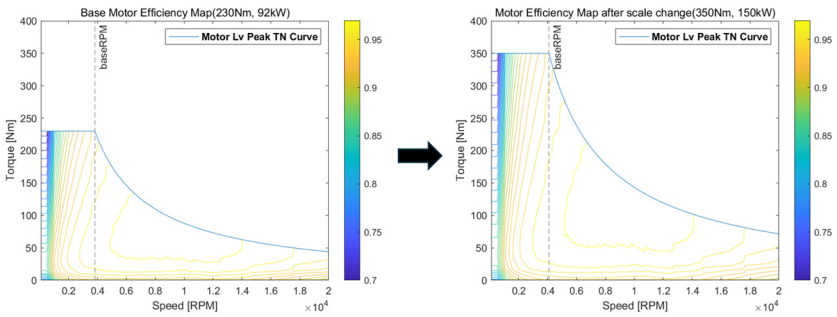

Figure 14. x, y-axis scale change in motor efficiency map.

It is essential to properly select the range of input variables during the training of a Neural Network to improve the quality of training data. In particular, the gear ratio

must be selected within a range that can satisfy the vehicle's required performance. This paper generated a baseline vehicle-level Peak Torque-Speed (T-N) Curve, which minimally satisfies the vehicle's required performance, to analyze whether the vehicle meets the required performance based on the powertrain specification combinations. The creation of the vehicle-level Peak T-N Curve was divided into two stages. First, the vehicle's top speed and maximum torque capable of climbing were calculated considering the driving resistance to reflect climbing performance and maximum speed, and a T-N Curve that meets these criteria was generated. However, the T-N Curve needed to be adjusted because the power required for acceleration performance is more significant than that needed for climbing performance or maximum speed. Therefore, a simple simulation was developed to check the time to reach 0–96 kph, and power was increased until the required acceleration performance was met, ultimately generating the Peak T-N Curve for performance requirement verification, as shown in Figure 15. This curve checks whether the vehicle satisfies the required performance based on different gear ratio combinations.

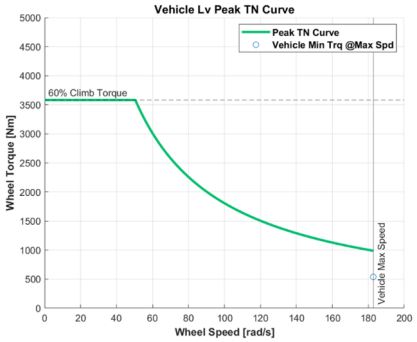

Figure 15. Peak T-N Curve for vehicle performance requirement verification.

4.1.2. Description of Adaptive Sampling Methods and Learning Techniques

The input variables are applied to a vehicle simulation to extract the time it takes to reach 0–96 kph and the change in SOC. The time to reach 96 kph is measured without following a driving cycle, with the accelerator pedal fixed at maximum until the vehicle speed reaches 96 kph. The change in SOC is reported as the final variation after running the driving cycle.

Simulations were conducted on various combinations of input variables to generate data for neural network training. However, if the training data contain only biased data, the model may converge but fail to simulate the entire dataset accurately. To prevent such bias in the training data, the range of each input variable was appropriately divided, and sampling was performed evenly using different combinations each time to avoid data bias. Additionally, the elementary effects method, commonly used to compare the impact of input variables on outputs, was employed. This method involves dividing the range of input variables that significantly impact the output into more segments while dividing those with less impact into fewer segments, thereby efficiently exploring the variable space. Additionally, generating training data requires many samples, and running simulations each time to extract data is time-consuming. Therefore, MATLAB Parallel Computing Toolbox was used to extract samples in parallel, reducing the sampling time.

Once a certain number of samples are collected, the training data are assembled, and training commences. Cross-validation was applied to calculate the model fitting error to prevent overfitting in the neural network and to assess the model's generalization ability more accurately. Initially, samples are divided into training sets and test sets according to a predetermined ratio. The training set is used for neural network training, while the test set compares the error between model estimates and actual values. The training and test sets are varied with each K-Fold split to calculate the fitting error, using the maximum error as the final fitting error. Normalized Root Mean Square Error (NRMSE) is the fitting error

metric used here. Figure 16 illustrates the process of extracting the fitting error through cross-validation.

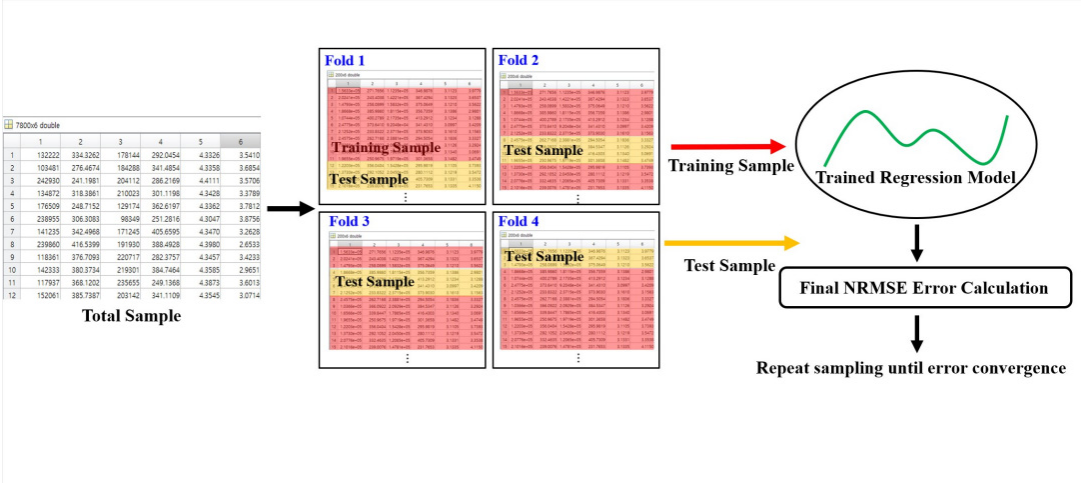

Figure 16. Schematic of model cross-validation and error calculation methods.

4.2. NSGA-II Based Multi-Objective Optimization

After determining the convergence of the neural network, the trained neural network model is used as the objective function for the optimization algorithm. It utilizes two objective functions: the change in SOC and the acceleration time (time to reach 0–96 kph). As there is a trade-off between acceleration performance and SOC change, it is necessary to explore solutions that best satisfy both objectives. NSGA-II is a multi-objective optimization algorithm often used when there is a need to optimize multiple conflicting objectives simultaneously [26]. Using this algorithm, a Pareto Front that maximizes acceleration performance and energy efficiency is explored, and weights are set between the two objectives to extract the optimal set of parameters.

$$\begin{cases} \underset{\Delta SOC}{minimize}\ f(M,\ R,\ V) \\ \underset{t_{acc}}{minimize}\ g(M,\ R,\ V) \end{cases} \tag{11}$$

$$subject\ to\ M, R, V\ \in\ \Omega_c$$

The objective functions f and g represent fully trained surrogate models, each designed to minimize the change in SOC and the acceleration time, respectively. $M = \left[T_{max_f},\ P_f,\ T_{max_r},\ P_r\right]$ denotes the set of input variables related to motor specifications, which includes the maximum torque of the front motor (T_{max_f}), power of the front motor (P_f), maximum torque of the rear motor (T_{max_r}), and power of the rear motor (P_r). $R = \left[r_f,\ r_{r_1}, r_{r_2}\right]$ represents the set of gear ratios, comprising the front gear ratio (r_f), the rear first gear ratio (r_{r_1}), and the rear second gear ratio (r_{r_2}). $V = [v_{1\to2}, v_{2\to1}]$ refers to the shifting speeds, including both the upshift speed ($v_{1\to2}$) and the downshift speed ($v_{2\to1}$). Finally, all input variables must be determined within the design specification range; therefore, constraints on the input variables (Ω_c) have been set in the optimization problem.

5. Results

Figure 17 shows the distribution of solutions for multi-objective optimization applied to three vehicle types—sedan, SUV, and SUV with trailer—during the WLTP driving cycle. The optimal solution set derived from the optimization algorithm, known as the Pareto Front, is represented by black dots, with specific solutions (A, B, C) indicated by red arrows on the Pareto Front. The optimization results are evaluated by comparing the change in SOC and acceleration performance between the reference vehicle parameter set and

the optimized parameter set under the WLTP driving cycle. Due to the characteristics of multi-objective optimization, the Pareto Front produces no clear superiority between the two objectives, and the optimal solution can vary depending on whether the focus is on energy efficiency or acceleration performance. This paper presents three types of optimal solutions by varying the weights given to acceleration performance or SOC change.

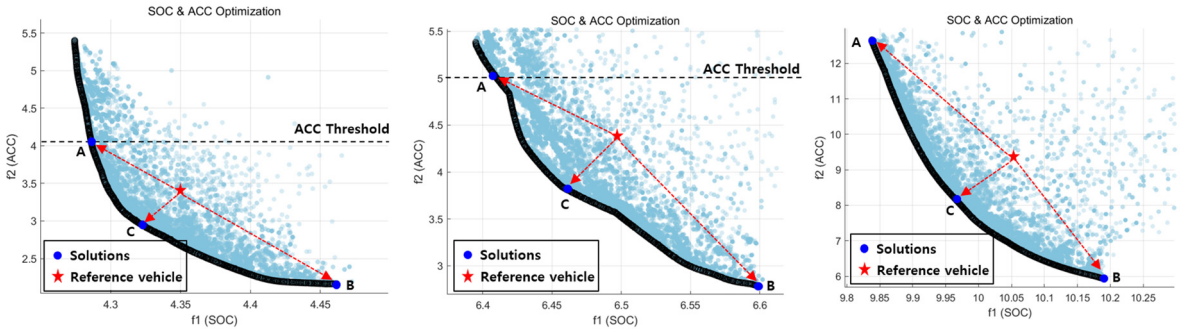

Figure 17. Optimization results for each vehicle specification under the WLTP cycle: Sedan (**left**), SUV (**middle**), and SUV with Trailer (**right**).

Firstly, solution A focuses solely on energy efficiency without considering acceleration performance. Thus, it selects the solution that minimizes the objective on the x-axis (SOC change) among the Pareto Front in Figure 17. Figure 17 displays a critical y-axis line (ACC Threshold) that excludes solutions not meeting the 0–96 km/h acceleration time criteria to reflect the required performance standards. Consequently, the critical value is established, and the solution with the minor SOC change that does not exceed this threshold is chosen as Solution A. Conversely, Solution B focuses on acceleration performance without considering energy efficiency. Hence, it represents the solution with the minimum y-axis (acceleration time) value on the Pareto Front. Solution C equally prioritizes acceleration performance and energy efficiency, carrying equal weight. Therefore, it is located between Solution A and B in the Pareto Front.

Additionally, validation across various driving cycles is necessary to enhance the generality and reliability of optimization results. Thus, results from another driving cycle, the US06 driving cycle, are further presented in Figure 18. Figures 19 and 20 display bar charts comparing the performance (ΔSOC, t_{acc}) of the Reference Vehicle and the optimized Solutions A, B, and C based on the WLTP driving cycle. These charts visually demonstrate the differences in SOC change and acceleration time for each solution, clearly representing the optimization's effectiveness. Additionally, Tables 3 and 4 show the changes in ΔSOC and the rates of change in acceleration performance for the Reference Vehicle when Solutions A, B, and C are applied, based on the WLTP cycle. Subsequently, the results from another driving cycle, the US06, are presented in Figures 21 and 22. Finally, Tables 5 and 6 depict the ΔSOC change and acceleration time change rates for the US06 cycle.

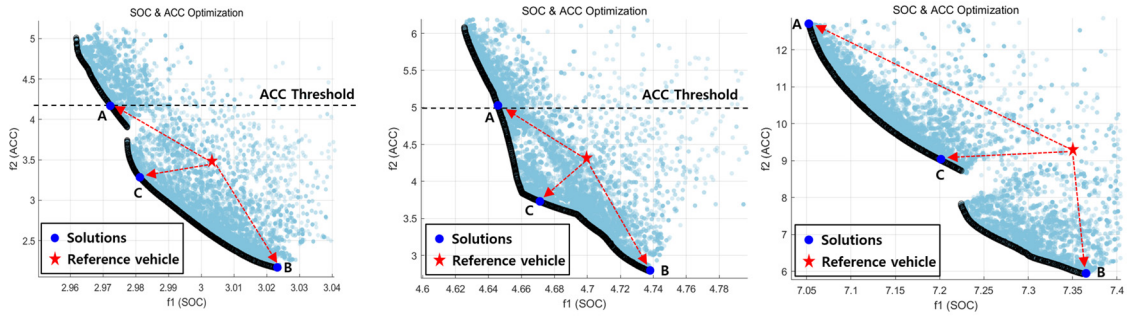

Figure 18. Optimization results for each vehicle specification under the US06 cycle: Sedan (**left**), SUV (**middle**), and SUV with Trailer (**right**).

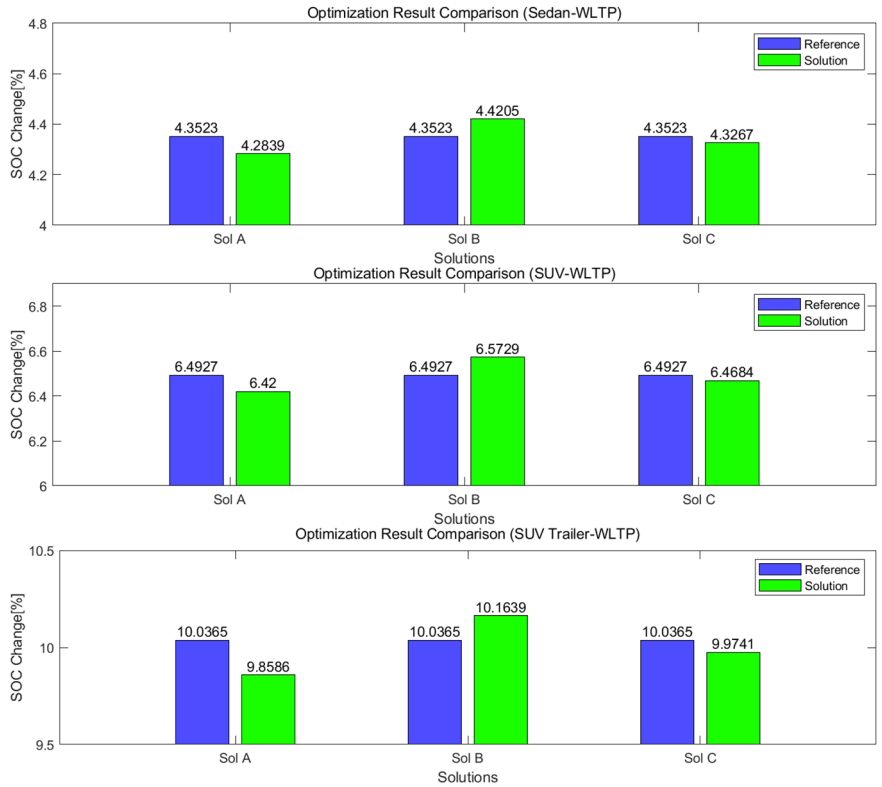

Figure 19. Comparison of SOC changes between the reference and each solution under the WLTP cycle: Sedan (**top**), SUV (**middle**), and SUV with Trailer (**bottom**).

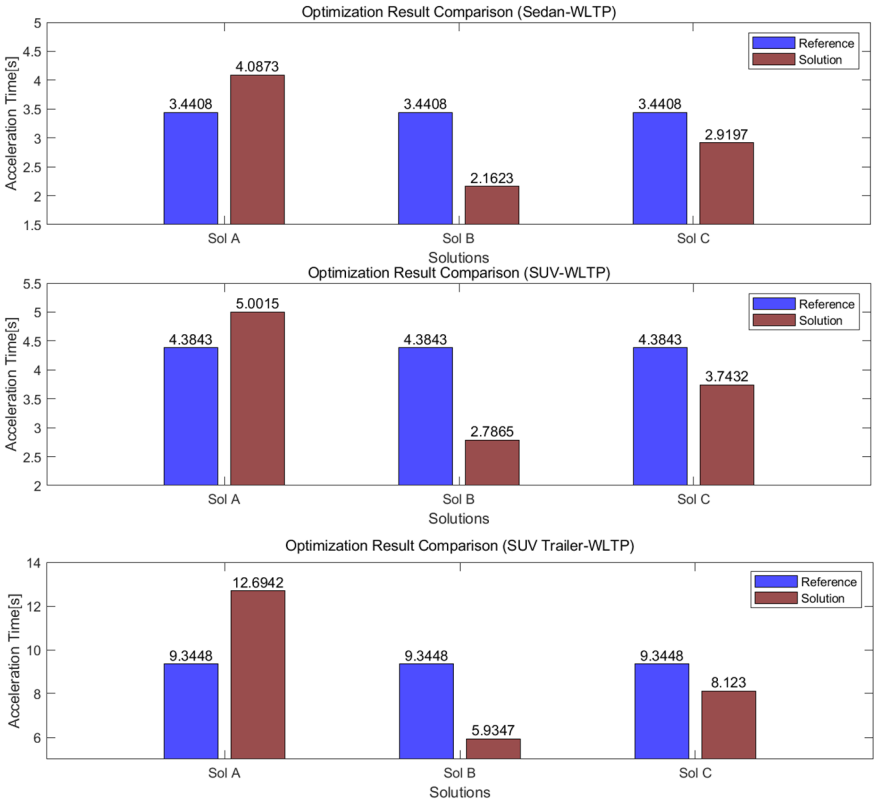

Figure 20. Comparison of acceleration time between the reference and each solution under the WLTP cycle: Sedan (**top**), SUV (**middle**), and SUV with Trailer (**bottom**).

Table 3. Rate of Change in SOC Following Optimization Applied to the Reference Vehicle (WLTP Drive Cycle).

Solution	Sedan	SUV	SUV-Trailer
A	−1.57%	−1.12%	−1.79%
B	1.56%	1.23%	1.29%
C	−0.58%	−0.37%	−0.56%

Table 4. Rate of Acceleration Time Following Optimization Applied to the Reference Vehicle (WLTP Drive Cycle).

Solution	Sedan	SUV	SUV-Trailer
A	18.8%	14.1%	35.7%
B	−37.2%	−36.4%	−36.5%
C	−15.1%	−14.6%	−13.1%

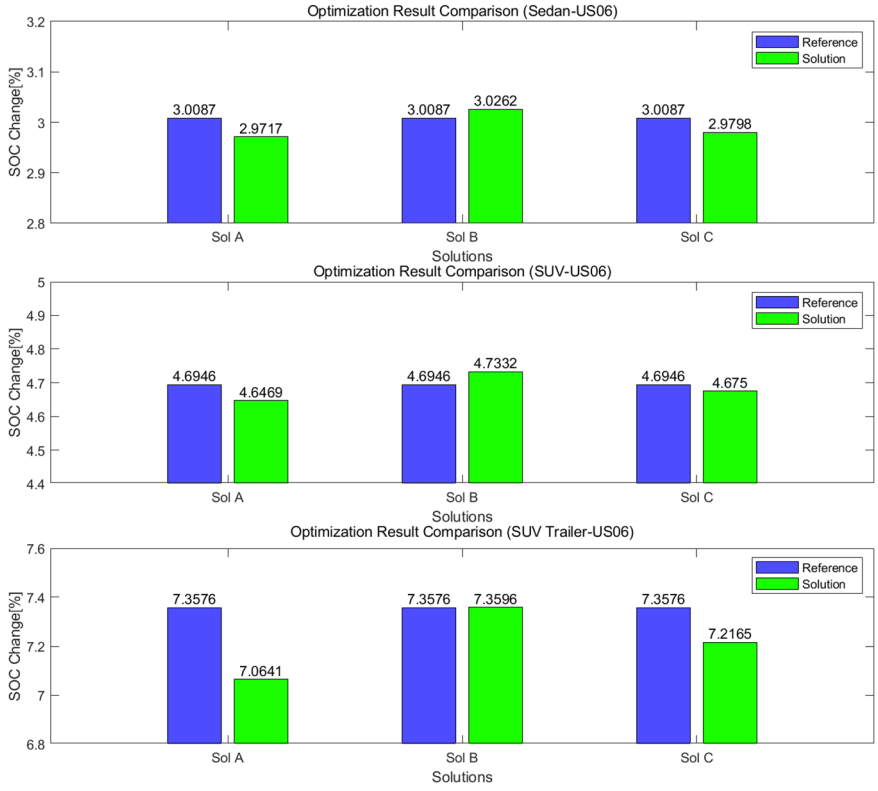

Figure 21. Comparison of SOC changes between the reference and each solution under the US06 cycle: Sedan (**top**), SUV (**middle**), and SUV with Trailer (**bottom**).

Table 5. Rate of Change in SOC Following Optimization Applied to the Reference Vehicle (US06 Drive Cycle).

Solution	Sedan	SUV	SUV-Trailer
A	−1.22%	−1.01%	−3.98%
B	0.58%	0.82%	0.01%
C	−0.96%	−0.41%	−1.91%

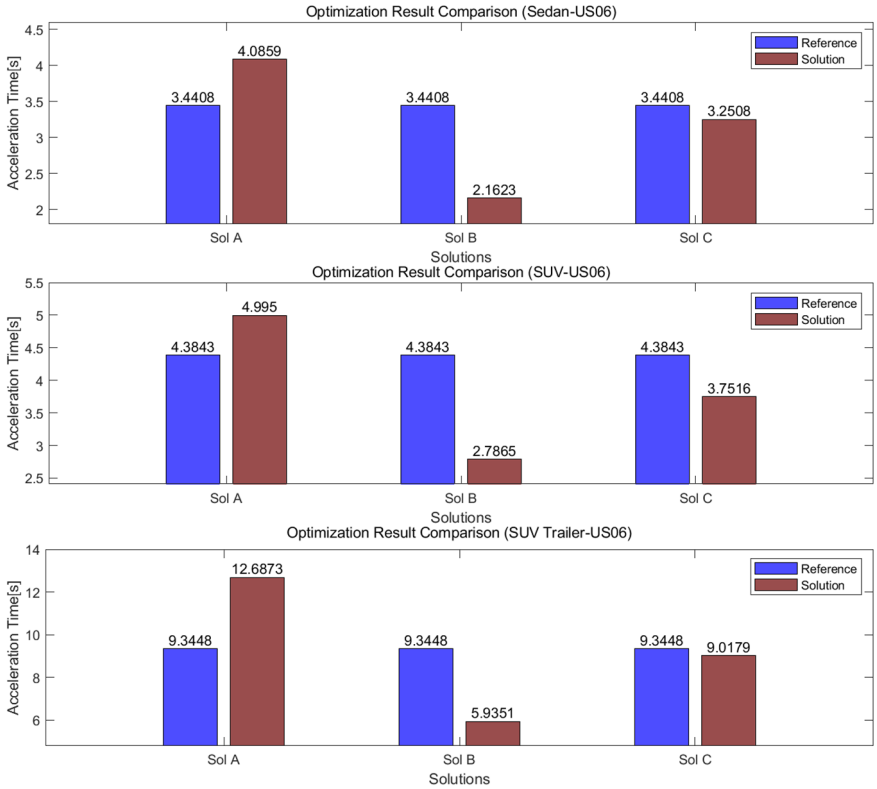

Figure 22. Comparison of acceleration time between the reference and each solution under US06 cycle: Sedan (**top**), SUV (**middle**), and SUV with Trailer (**bottom**).

Table 6. Rate of Acceleration Time Following Optimization Applied to the Reference Vehicle (US06 Drive Cycle).

Solution	Sedan	SUV	SUV-Trailer
A	18.7%	13.9%	35.7%
B	−37.1%	−36.4%	−36.4%
C	−5.52%	−14.4%	−3.49%

Solution A aims to maximize energy efficiency, which, as shown in Table 3, significantly reduces the SOC changes. However, as seen in Table 4, it conversely increases in acceleration time. On the other hand, Solution B focuses on acceleration performance, leading to an increase in SOC changes while significantly decreasing acceleration time. Solution C balances the two objectives, reducing SOC changes and acceleration time compared to the reference vehicle. The application of Solution C results in a decrease in SOC changes by 0.58% (Sedan), 0.37% (SUV), and 0.56% (SUV-Trailer), and a reduction in 0–96 kph acceleration time by 15.1% (Sedan), 14.6% (SUV), and 13.1% (SUV-Trailer). Additionally, as shown in Tables 5 and 6, the US06 driving cycle demonstrates similar patterns of change when the optimization results are applied, comparable to the WLTP driving cycle. Figures 23 and 24 present examples of the results from applying Solutions A, B, and C to vehicle simulations. Each figure compares the SOC change and vehicle speed over time between the Reference Vehicle and Solutions A, B, and C. In terms of energy consumption (Figure 23), Solution A achieved the best results, while Solution B showed the best results in acceleration performance (Figure 24).

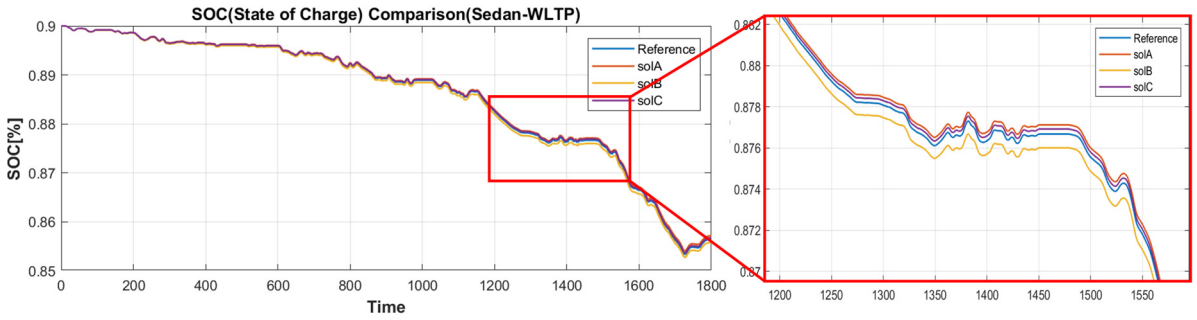

Figure 23. Results from Applying Optimized Solutions to Vehicle Simulations for Comparison: SOC.

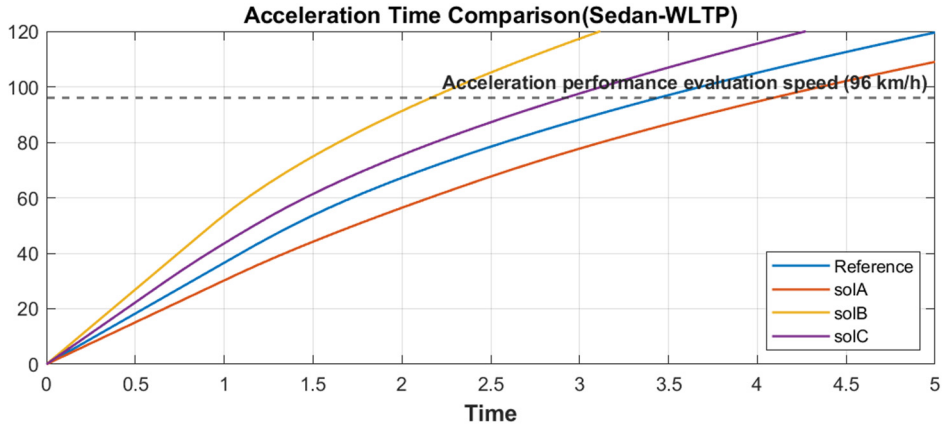

Figure 24. Results from Applying Optimized Solutions to Vehicle Simulations for Comparison: Acceleration Time.

6. Conclusions

This study presented a torque distribution strategy using fuzzy logic and multi-objective optimization based on surrogate models to determine the optimal powertrain component specifications for an AWD powertrain structure with a two-stage gearbox in the rear. Electric vehicle modeling was conducted using MATLAB/Simulink, which included a torque compensation method to prevent torque holes during shifting and a speed synchronization process considering the neutral state of the rear motor.

Additionally, using fuzzy theory, the method proposed an adjustment between the torque distribution strategies based on motor efficiency maps and the distribution strategies considering driving stability in driving and braking situations. Subsequently, a vehicle-level Peak T-N Curve was generated considering performance indicators, and performance was comprehensively reviewed. Neural network training was conducted through MATLAB parallel simulation, and a surrogate model-based optimization objective function was created. Finally, NSGA-II multi-objective optimization was carried out to generate a set of solutions that considered both energy efficiency and acceleration performance. In the solution set, optimal solutions can be derived by setting weights for the two objectives to reflect their importance. This paper presents examples of solutions that consider only energy efficiency, only acceleration performance, and solutions that assign equal weights to both objectives. When equal weights were assigned, SOC change improved by 0.37~0.58%, and acceleration performance improved by 13.1~15.1%.

However, the improvement in SOC change from the optimization results was insignificant, which can be attributed to the main factor determining energy efficiency in the simulation, the baseline motor efficiency map. The efficiency map used in the study showed little difference in motor efficiency outside the low-torque and low-speed areas. Thus, even with changes in the motor operating points within the efficiency map, the efficiency variation was minimal, leading to no significant difference in SOC change. If there

were apparent differences in efficiency with changes in torque and speed in the baseline motor efficiency map, applying the optimization results from this study would result in more significant improvements in energy efficiency.

Author Contributions: Conceptualization, J.K., J.A., Y.-G.P. and D.C.; software, J.K., J.A. and Y.-G.P.; validation, J.K.; formal analysis, J.K., J.A., S.J., Y.-G.P. and H.K.; investigation, J.K., J.A. and S.J.; data curation, J.K.; writing, J.K.; visualization, J.K.; supervision, S.-H.H.; funding acquisition, S.-H.H. All authors have read and agreed to the published version of the manuscript.

Funding: This paper was supported by the Korea Institute for Advancement of Technology (KIAT) grant funded by the Korean Government (MOTIE) (P0017120, The Competency Development Program for Industry Specialist). This work was supported by the Technology Innovation Program (or Industrial Strategic Technology Development Program—Development of Infotainment Technology and Service Demonstration based on Automated Shuttle) (20014983, Development of autonomous chassis platform for a modular vehicle) funded By the Ministry of Trade, Industry and Energy (MOTIE, Republic of Korea).

Data Availability Statement: The original contributions presented in the study are included in the article, further inquiries can be directed to the corresponding author.

Acknowledgments: This study originates from an EVS37 poster presentation in Seoul, South Korea (24 April 2024). Special thanks to the EVS37 program for the opportunity to submit this research paper to this WEVJ Special Issue.

Conflicts of Interest: The authors declare no conflicts of interest.

References

1. Lutsey, N. Global climate change mitigation potential from a transition to electric vehicles. *Int. Counc. Clean Transp.* **2015**, *2015*, 5.
2. Bryhadyr, I.; Panova, I.; Strelianyi, V. Transition from internal combustion engines to electric motors–legal and organizational dimensions. *Stud. Nad Bezpieczeństwem* **2021**, *6*, 77–85.
3. Das, P.K.; Bhat, M.Y. Global electric vehicle adoption: Implementation and policy implications for India. *Environ. Sci. Pollut. Res.* **2022**, *29*, 40612–40622. [CrossRef] [PubMed]
4. Muratori, M.; Alexander, M.; Arent, D.; Bazilian, M.; Cazzola, P.; Dede, E.M.; Farrell, J.; Gearhart, C.; Greene, D.; Jenn, A.; et al. The rise of electric vehicles—2020 status and future expectations. *Prog. Energy* **2021**, *3*, 022002. [CrossRef]
5. Wang, J.; Zhang, C.; Guo, D.; Yang, F.; Zhang, Z.; Zhao, M. Drive-Cycle-Based Configuration Design and Energy Efficiency Analysis of Dual-Motor 4WD System with Two-Speed Transmission for Electric Vehicles. *IEEE Trans. Transp. Electrif.* **2023**, *10*, 1887–1899. [CrossRef]
6. El Hadraoui, H.; Zegrari, M.; Chebak, A.; Laayati, O.; Guennouni, N. A multi-criteria analysis and trends of electric motors for electric vehicles. *World Electr. Veh. J.* **2022**, *13*, 65. [CrossRef]
7. Ruan, J.; Song, Q. A novel dual-motor two-speed direct drive battery electric vehicle drivetrain. *IEEE Access* **2019**, *7*, 54330–54342. [CrossRef]
8. Huang, W.; Huang, J.; Yin, C. Optimal design and control of a two-speed planetary gear automatic transmission for electric vehicle. *Appl. Sci.* **2020**, *10*, 6612. [CrossRef]
9. Janulin, M.; Vrublevskyi, O.; Prokhorenko, A. Energy minimization in city electric vehicle using optimized multi-speed transmission. *Int. J. Automot. Mech. Eng.* **2022**, *19*, 9721–9733. [CrossRef]
10. Odrigo, A. Development of Multi-Wheel Drivetrain Control System for Future Electric Combat Vehicle. Ph.D. Thesis, University of Ontario Institute of Technology, Oshawa, ON, Canada, 2017.
11. Dizqah, A.M.; Lenzo, B.; Sorniotti, A.; Gruber, P.; Fallah, S.; De Smet, J. A fast and parametric torque distribution strategy for four-wheel-drive energy-efficient electric vehicles. *IEEE Trans. Ind. Electron.* **2016**, *63*, 4367–4376. [CrossRef]
12. Cao, K.; Hu, M.; Wang, D.; Qiao, S.; Guo, C.; Fu, C.; Zhou, A. All-wheel-drive torque distribution strategy for electric vehicle optimal efficiency considering tire slip. *IEEE Access* **2021**, *9*, 25245–25257. [CrossRef]
13. Kim, K.; Kim, N.; Jeong, J.; Min, S.; Yang, H.; Vijayagopal, R.; Cha, S.W. A Component-Sizing Methodology for a Hybrid Electric Vehicle Using an Optimization Algorithm. *Energies* **2021**, *14*, 3147. [CrossRef]
14. Nguyen, C.T.; Walker, P.D.; Zhou, S.; Zhang, N. Optimal sizing and energy management of an electric vehicle powertrain equipped with two motors and multi-gear ratios. *Mech. Mach. Theory* **2022**, *167*, 104513. [CrossRef]
15. Delavaux, M.; Lhomme, W.; McGordon, A. Comparison between forward and backward approaches for the simulation of an electric vehicle. In Proceedings of the IEEE Vehicle Power and Propulsion Conference (VPPC2010), Lille, France, 1–3 September 2010; pp. 3–5.
16. Viadero-Monasterio, F.; Meléndez-Useros, M.; Jiménez-Salas, M.; Boada, B.L. Robust Adaptive Heterogeneous Vehicle Platoon Control Based on Disturbances Estimation and Compensation. *IEEE Access* **2024**, *12*, 96924–96935. [CrossRef]

17. Choi, W. A Study on Mode Conversion Control of the Power Distribution System of Dual Motors Equipped Electric Vehicle. Ph.D. Thesis, Seoul National University of Science and Technology, Seoul, Republic of Korea, 2023.
18. De Pinto, S.; Camocardi, P.; Sorniotti, A.; Gruber, P.; Perlo, P.; Viotto, F. Torque-fill control and energy management for a four-wheel-drive electric vehicle layout with two-speed transmissions. *IEEE Trans. Ind. Appl.* **2016**, *53*, 447–458. [CrossRef]
19. Park, J.; Jeong, H.; Jang, I.G.; Hwang, S.H. Torque distribution algorithm for an independently driven electric vehicle using a fuzzy control method. *Energies* **2015**, *8*, 8537–8561. [CrossRef]
20. Fajri, P.; Lee, S.; Prabhala, V.A.K.; Ferdowsi, M. Modeling and integration of electric vehicle regenerative and friction braking for motor/dynamometer test bench emulation. *IEEE Trans. Veh. Technol.* **2015**, *65*, 4264–4273. [CrossRef]
21. Kumar, C.S.N.; Subramanian, S.C. Cooperative control of regenerative braking and friction braking for a hybrid electric vehicle. *Proc. Inst. Mech. Eng. Part D J. Automob. Eng.* **2016**, *230*, 103–116. [CrossRef]
22. Lin, X.; Lin, Z.; Wei, S. Multi-objective optimized driving strategy of dual-motor EVs using NSGA-II as a case study and comparison of various intelligent algorithms. *Appl. Soft Comput.* **2021**, *111*, 107684. [CrossRef]
23. Kwon, K.; Lee, J.H.; Lim, S.K. Optimization of multi-speed transmission for electric vehicles based on electrical and mechanical efficiency analysis. *Appl. Energy* **2023**, *342*, 121203. [CrossRef]
24. Lartaud, P.; Humbert, P.; Garnier, J. Sequential design for surrogate modeling in Bayesian inverse problems. *arXiv* **2024**, arXiv:2402.16520.
25. Dasi, M.; Thoma, P. Surrogate Modelling for S-Parameters by Using State Space Mapping. In Proceedings of the 2023 International Conference on Electromagnetics in Advanced Applications (ICEAA), Venice, Italy, 9–13 October 2023; IEEE: Piscataway, NJ, USA, 2023; p. 75.
26. Deb, K. Multi-objective optimisation using evolutionary algorithms: An introduction. In *Multi-Objective Evolutionary Optimisation for Product Design and Manufacturing*; Springer: London, UK, 2011; pp. 3–34.